Nuclear Engineering and Technology 54 (2022) 4759–4775

Contents lists available at ScienceDirect

Nuclear Engineering and Technology

journal homepage: www.elsevier.com/locate/net

Original Article

Application of two different similarity laws for the RVACS design

Min Ho Lee [a], Ji Hwan Hwang [b], Ki Hyun Choi [b], Dong Wook Jerng [b, **], In Cheol Bang [a, *]

[a] Department of Nuclear Engineering Ulsan National Institute of Science and Technology (UNIST) 50 UNIST-gil, Ulju-gun, Ulsan, 44919, Republic of Korea
[b] School of Energy Systems Engineering Chung Ang University 84 Heukseok-ro, Dongjak-gu, Seoul, 06974, Republic of Korea

ARTICLE INFO

Article history:
Received 25 May 2022
Received in revised form
21 July 2022
Accepted 30 July 2022
Available online 17 August 2022

Keywords:
RVACS
SFR
Passive safety
Natural circulation
Liquid metal
Similarity law

ABSTRACT

The RVACS is a versatile and robust safety system driven by two natural circulations: in-vessel coolant and ex-vessel air. To observe interaction between the two natural circulations, SINCRO-IT facility was designed with two different similarity laws simultaneously. Bo' based similarity law was employed for the in-vessel, while Ishii's similarity law for the ex-vessel excluding the radiation. Compared to the prototype, the sodium and air system, SINCRO-IT was designed with Wood's metal and air, having 1:4 of the length reduction, and 1.68:1 of the time scale ratio. For the steady state, RV temperature limit was violated at 0.8% of the decay heat, while the sodium boiling was predicted at 1.3%. It showed good accordance with the system code, TRACE. For an arbitrary re-criticality scenario with RVACS solitary operation, sodium boiling was predicted at 25,100 s after power increase from 1.0 to 2.0%, while the system code showed 30,300. Maximum temperature discrepancy between the experiments and system code was 4.2%. The design and methodology were validated by the system code TRACE in terms of the convection, and simultaneously, the system code was validated against the simulating experiments SINCRO-IT. The validated RVACS model could be imported to further accident analysis.

1. Introduction

The natural circulation phenomena can transport fluid without pumping or blowing. Therefore, natural circulation is important for passive safety of the nuclear reactor, which could secure cooling without power. As passiveness of the nuclear safety system is emphasized, various safety systems were developed based on the natural circulation. Regard to water-cooled reactor, it includes phase change for more effective heat removal. The advanced passive pressurized water reactor (AP 1000) has a passive residual heat removal heat exchanger (PRHR HX), which is a part of natural circulation loop [1], and passive containment cooling system (PCCS) is operating based on the natural circulation [2]. Different to water-cooled reactors, Gen-IV reactors do not allow phase change of the coolant. Therefore, safety systems of the Gen-IV reactors have been developed based on the single-phase natural circulation, especially for liquid metal-cooled fast reactors (LMRs).

Regard to loop type LMRs, there is no space for decay heat removal systems (DHRSs) in the primary vessel, so that the DHRSs are not located at the primary side of the plant. Japanese sodium-cooled fast reactor (SFR) Joyo had dump heat exchangers in the intermediate loop, and the decay heat removed through the natural circulation of the primary and intermediate loop [3]. Another Japanese SFR MONJU has a similar DHRS, which is called passive reactor auxiliary cooling system (PRACS), which is located at the intermediate loop. In addition, the MONJU could employ direct reactor auxiliary cooling system (DRACS) inside of the reactor vessel thanks to relatively large vessel [4]. For developing pool type SFR, ASTRID, there are three decay heat removal systems: RRA, RRB, and RRC. Among them, the RRB is a natural circulation loop with direct heat exchanger in the pool, and air heat exchanger [5]. The prototype gen-IV SFR (PGSFR), which is under development in Korea Atomic Energy Research Institute (KAERI), has active and passive decay heat removal system in the pool, as active decay heat removal system, (ADHRS) and passive DHRS (PDHRS), which are similar to RRA and RRB in the ASTRID [6]. Different to SFR, lead-cooled fast reactors (LFRs) were pool type reactor, and most of them employed DHX in the pool, such as ELFR, BREST-OD-300, ALFRED, and MYRRHA [7–9].

Most of the natural circulation driven systems could be evaluated analyzing a single natural circulation loop. For example, submerged type heat exchanger could be simplified as loop with a submerged heat exchanger as a heater, and the other heat

* Corresponding author.
** Corresponding author.
E-mail addresses: dwjerng@cau.ac.kr (D.W. Jerng), icbang@unist.ac.kr (I.C. Bang).

https://doi.org/10.1016/j.net.2022.07.023

exchanger as a cooler. Boundary condition of the heater and cooler could be characterized as flow condition of the external side of the heat exchangers. The external flow conditions are treated as secondary inlet condition of the heat exchanger, therefore, internal natural circulation do not significantly interact with external flow. Even for the natural circulation in the intermediate loop, which could be observed in JOYO and MONJU, it is relatively simple because it occurs in the loop.

However, the RVACS, which is an abbreviation of the reactor vessel auxiliary cooling system, has unique heat transfer characteristics compared to the other decay heat removal systems. As shown in Fig. 1, decay heat from the core is transferred from the core to the reactor vessel (RV), via in-vessel natural circulation of the coolant. Then, heat is finally transferred to the ultimate heat sink air, from the RV by ex-vessel natural circulation of the air. Therefore, two natural circulations are conjugated, and interact each other. Cooling boundary of the in-vessel corresponds to the heating boundary of the ex-vessel. Change of the temperature or heat flux distribution of one side could affect to the natural circulation characteristics of the other side. It is very important especially in transient, and it is the most unique characteristics of the RVACS.

Regard to the in-vessel natural circulation, experiments were mainly conducted with simulant, due to advantages of scale reduction and difficulties of handling with liquid metals. Similarity of natural circulation was suggested by Grewal et al. and water showed better temperature accordance than sodium in small scale facility [10]. The similarity law was validated by numerical [11], and experimental method [12]. Error in the water simulation experiment was 7–30 % in numerical validation, and 27% in maximum in experimental validation, respectively. Based on the similarity law, most of the experiments were conducted with water as a simulant of the sodium. RAMONA and NEPTUN facilities were designed to analyze natural circulation under DHX operation, and complex natural circulation flow was observed in the hot pool due to countercurrent flow at the upper plenum [13,14]. In the PHEASANT facility, particle image velocimetry was used to observe natural circulation flow and temperature transient [15].

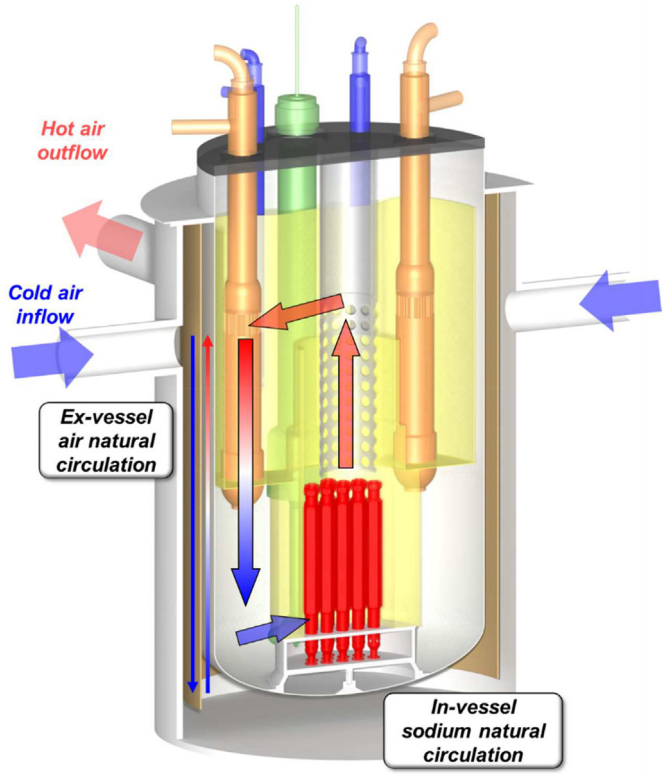

Fig. 1. Schematic of the RVACS

For ex-vessel natural circulation, air was used in the experiments in common due to its favorable characteristics for experiments. It could be characterized as natural convection in the vertical channel with heating from two walls facing each other. Heat transfer correlations based on Rayleigh number (Ra) have been suggested by various researcher in that condition [16–18]. For PRISM and SAFR, which are RVACS applied SFRs, RVACS performance was experimentally evaluated. and heat transfer correlation was developed [19]. In the very similar geometry from the very high temperature gas-cooled reactor (VHTR), flow was visualized using particle imaged velocimetry [20]. An experimental facility for RVACS in PGSFR was developed [21], and empirical correlation based on Ra with development of rising flow [22,23].

Integrated analyses were conducted with mainly system code. RVACS in the small lead-cooled fast reactor (LFR) was analyzed using RELAP5, and basic parametric studies on chimney height and vessel size were conducted [24]. RVACS in the PGSFR was analyzed, focusing on real-time system response [25]. Heat removal by RVACS approached to the decay heat as time goes by, however, its activation time is important for safe time of temperature of internal structures. For Chinese SFR, a THACS code employed to analyze performance of RVACS performance, and in-vessel natural circulation showed good accordance with the experiments predicting reverse flow [26].

Performance analysis of the RVACS requires integrated and transient analysis considering progress of accident. Due to complex reactivity feedback and scale of the system, the system code is the best tool for accident analysis. However, the system codes were validated against limited, separated cases in so far. There is no integrated and transient experimental database for strict validation. Therefore, in present study, an experimental facility was designed to analyze performance of the RVACS in transient and integrated manner based on the combination of the two different similarity laws, which has never been endeavored so far. Both steady state and transient conditions were experimentally, and numerically analyzed. Time of occurrence of sodium boiling anticipated by the simulating experiment showed good accordance with the results from the system code.

2. Design of an experimental facility, SINCRO-IT

An experimental facility named SINCRO-IT was designed to conduct integrated and transient experiment for the RVACS. It is an abbreviation of simulating natural circulation under RVACS operation – integrated and transient. It was designed based on the PGSFR, using two different similarity law for in- and ex-vessel. It was the most important and unique point in the current experiment. Different similarity law was applied to the in- and ex-vessel side in a single facility. Overall process from its conceptual design to detailed discussions on the combination of the two different similarity laws would be discussed in detail.

2.1. Conceptual design

Experimental facility was simplified as 2-D to focus on the interaction of both sides. It could be divided into Wood's metal pool, which corresponds to in-vessel, and air-cooling channel, which corresponds to ex-vessel. As it is simplified as 2-D, it is important to select proper cross section of original 3-D prototype. Especially, cold pool surrounding the redan, the IHX, and inlet

piping were simplified. For the PGSFR, coolant flows in the same way to normal operation: core – upper plenum – intermediate heat exchanger (IHX) – lower plenum – inlet piping – core inlet. Therefore, it was set as a cross section including IHX with in-vessel structures. To separate core and lower plenum like core shroud, and to separate the upper plenum and lower plenum like redan, a partition was introduced as an orange wall in Fig. 2. The cold pool surrounding the redan was neglected because this narrow cold pool between the RV and redan could make solidification problem and distortion in the similarities. IHX was reflected into the design as HX for normal operation without its shell, which is blue pipe. It was installed to simulate heat removal of IHX during normal operation, however, it was not used in the test. Inlet piping and pump were not reflected into the SINCRO-IT because the experiments were focusing on the natural circulation. Core was simulated as a group of cartridge heaters, on the bottom-right of the figure. The pool was only cooled by attached air-cooling channel.

Regard to ex-vessel, air-cooling was simulated by a single rising channel like gold square channel in Fig. 2, which was simplified from channel including descending and rising in Fig. 1. Therefore, separator between descending and rising channel was also omitted.

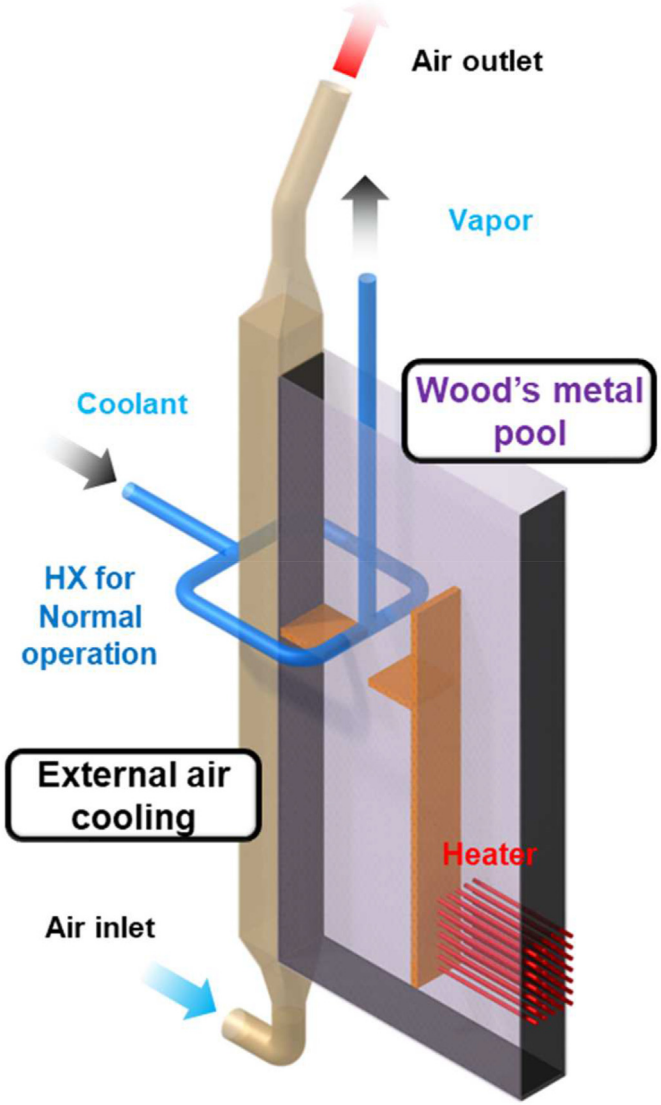

Fig. 2. Schematic of the SINCRO-IT

Different to prototype, which has a height and temperature difference enough to supply sufficient pressure head for natural circulation, in the SINCRO-IT, flow was simulated as forced circulation with equivalent flow rate. In the prototype, air is heated by the vessel and simultaneously heated by separator at the opposite side due to radiation. However, it was simplified by single wall heating because radiation is omitted due to temperature limitation. The SINCRO-IT was designed only considering the convective heat transfer.

Because the radiation was out of scope, the original double vessels (RV and containment vessel, CV) were simplified as a single wall. In the low temperature range, the radiation could not be properly simulated. In addition, it was hard to remove conduction between the two vessels, in the two-dimensional, simplified geometry. Although the two vessels and gap are properly designed, has no special functions in terms of heat transfer. They act like a damper for both spatial and transient point of view, like flattening of the temperature distribution through the gap, and delay of the transient. Therefore, the double vessels were simplified as a single wall, like Fig. 2.

2.2. Time scale and simulant

Keys for the integrated experimental facility are a combination of two different similarity law, and an identical time scale for in- and ex-vessel. With disagreed time scale for in- and ex-vessel, transient experiment could not be conducted. The time scale represents that speed of time flow in the scaled domain compared to the real-time. Time scale ratio 2 means that time in the experiment is scaled 1 to 2. In other words, time flow in the experiment is 2 times slower than the real time. Thus, in-vessel time scale was larger than that of the ex-vessel side, it means that in-vessel time flew slower than ex-vessel time. Therefore, time scale should match each other, and the time scale is the most important thing in the current scaling methods: the combination of the two different similarity laws for different domains. In this section, process of making time scales identical, and selection of the simulants for each domain were discussed. Detailed design for each side of the vessel would be discussed later.

Time scale in the modified Boussinesq number (Bo') based similarity law, which is applied for in-vessel natural circulation, is summarized in equation (1). Isometric scaling was applied in the Bo' based law, while ex-vessel Ishii's similarity law has anisotropy. Equation (2) is time scale of fluid and (3) is that of the solid. For the solid time scale, it is hard to be meaningful because double walled vessel was already simplified as a single wall. Therefore, it was omitted in further discussions. Length scale was divided into length along flow direction L, and thickness of the flow channel d. The two time scales have many thing in common, however, due to this anisotropy of Ishii's law, a time scale could be adjusted.

$$t_{ref,R} = \left\{ \left(\frac{\rho c_p L^4}{\beta g} \right)^{1/3} Q^{-1/3} \right\}_R \tag{1}$$

$$t_{f,R} = \left\{ \left(\frac{\rho c_p d L}{2 \beta g q''} \right)^{1/3} \right\}_R \tag{2}$$

$$t_{s,R} = \left(\frac{\alpha_s}{\delta_s^2} \frac{L}{u_{ref}} \right)_R \tag{3}$$

Regard to in-vessel, original fluid was sodium, and simulants were considered in this section. Fig. 3 is a relative length scale to

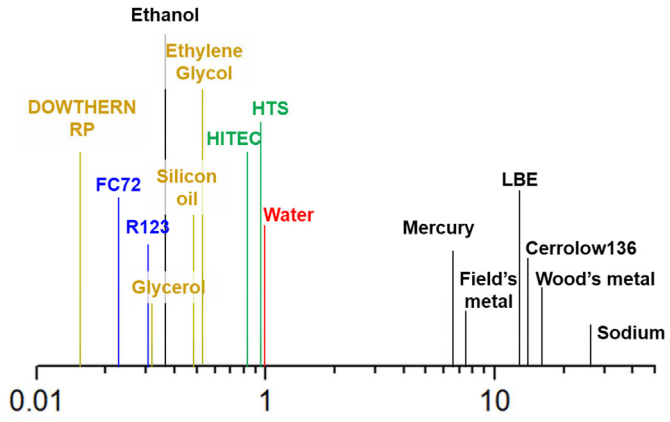

Fig. 3. Relative length scale for identical Bo'.

have identical Bo', under same volumetric heat generation rate. Water was set as a standard, 1. As fluids are located more right on the number line, the system should have bigger size to have Bo' similarity. For example, to simulate a Field's metal having 7.5 on the number line, by HITEC having 0.85, the HITEC system should be reduced from the Field's metal system by 0.85–7.5 (1–8.8) in terms of the length scale. It could guarantee identical Bo' between the two systems.

Considering a simulant of sodium, it could be divided into two groups. One group is liquid metals, having relatively larger scale than non-metallic fluids. Considering scale difference between the sodium and the group, simulating system would be several times smaller than the original facility. Among the group, mercury was excluded for safety and its toxicity, and Field's metal was also excluded for its high cost, due to its one expensive element, indium. Among the three candidates, which were mainly composed of bismuth and lead, LBE was excluded due to its higher melting point than Cerrolow136 and Wood's metal. Finally, Wood's metal was selected as a representative for a metallic simulant of sodium due to its operation experience. The other group is non-metallic fluids. Among them, other fluids have many disadvantages in terms of cost, safety, handling, and experience, compared with water. Therefore, many researches used the water as a non-metallic simulant of sodium [9–15]. Between the water and sodium, there are 25 times of the scale difference, thus, water facility should be reduced from its original system quite large. In short, metallic simulant, Wood's metal requires small scale reduction to the original system, while water requires more scale reduction. The scale of the experimental facility would be discussed with time scale in the following table.

Table 1 summarize characteristics of the simulant candidates of sodium. The time scale ratios were determined with proper length scale reduction depending on the simulant with compromise of Bo' in a reasonable range. Regard to water, its time scale was 1.24 at 1/10 of scale reduction, which means time flow in the experimental facility is 1.24 times slower than actual time, while that of the Wood's metal was 1.86 at 1/3 of scale reduction. Pros and cons of the water are opposite to that of the Wood's metal. Water is the most familiar fluid, and its properties and characteristics were known well. It is very inexpensive as well. However, considering its boiling point, it should be maintained lower than 100°C, so that overall temperature and heat flux would be limited to remain as a single-phase. Among the elements of the Wood's metal, Cadmium has the lowest boiling point as 760°C. Therefore, Wood's metal could be easily maintained in single phase without significant concern for its boiling. Since scaling difference with original simulant sodium is small, geometry of the original system could be reflected into the experimental facility in detail. However, freezing point of the Wood's metal is approximately 70°C, therefore, temperature of the facility should be maintained above freezing of the Wood's metal.

Table 2 shows characteristics of ex-vessel working fluid. The time scale ratios were calculated with proper length scale reduction and heat flux from the heating surface depending on the simulant with reasonable accordance of heat transfer similarity. Water and air were considered as simulant for the air. Since air is already gas, it could be maintained single-phase always, with relatively lower system power. However, due to low heat transfer coefficient (HTC) of the air, system temperature would be relatively higher than the water-cooled system. In case of water as simulant of air, the experimental facility could be smaller than that of the air with lower system temperatures. The time scale ratios were 1.60 in the air, while 0.41 in the water. As shown in equation (2), all parameters were reflected into the final time ratio as a power of 1/3, the time scale ratio do not change remarkably with change of parameters. Therefore, in terms of the accordance of the two time scale between in- and ex-vessel, time scale of ex-vessel should be a standard.

Considering scaling ratio and characteristics of the in- and ex-vessel simulants, Wood's metal / water combination is hard to be realized due to contrary temperature limits; solidification of the Wood's metal and boiling of water. Regard to water / air combination, air cooling has not enough coolability to maintain inner water under boiling, even with high power for in-vessel similarity. In case of water / water combination, they showed good accordance in terms of temperature, coolability, and system scale. Good coolability of the water convection could provide enough cooling to keep in-vessel water from boiling. However, time scaling ratios were quite different as 1.24 and 0.41 for in- and ex-vessel, respectively. This gap could not be closed by system parameter change.

Therefore, Wood's metal / air combination is the best and only solution for the integrated RVACS experiments. The Wood's metal requires high temperature to prevent freezing, and it could be easily achieved by low heat transfer performance of the external air. Proper power for similarity also showed similar magnitude for both in- and ex-vessel. The most important parameter, time scale, is 1.86 and 1.60 for in- and ex-vessel respectively. It could be matched easily by manipulating parameters within reasonable similarity range. As a result of simulant consideration, Wood's metal / air combination was selected as simulant for the integrated RVACS experiments, and similarity would be discussed in the following parts.

Table 1
Comparison between Wood's metal and water as simulant of sodium.

Material	Water	Wood's metal
Advantages	Easy handling Cost efficient	No boiling Less scale reduction
Disadvantages	Boiling problem → limitation for maximum temperature and heat flux	Solidification problem → limitation for the minimum temperature
Time scale ratio	1.24 (@ 1/10 scale)	1.86 (@ 1/3 scale)

Table 2
Comparison between air and water as simulant of air.

Material	Air	Water
Advantages	Always single phase Relatively lower power	Small system Low system temperature
Disadvantages	Large system required High system temperature	Boiling problem → limitation for maximum temperature and heat flux Require high power
Time scale ratio	1.60 (@ 1/5 scale, 1 kW/m^2)	0.41 (@ 1/10 scale, 20 kW/m^2)

2.3. In-vessel similarity law

The modified Boussinesq number (Bo') is the key for in-vessel similarity. It was derived from non-dimensionalization of the three governing equations like equation (4) – (6). In the diffusion terms of the non-dimensionalized momentum and energy equation, there are two non-dimensional numbers were derived. The modified Grashof number (Gr') is summarized in equation (7), and it means the ratio of the buoyant potential to viscous force. The most important number, Bo' is summarized in equation (8). It represents the ratio of heat transferred by the natural circulation to conduction in the aspect of the system. Larger Bo' means heat is mainly transferred as natural circulation than conduction. The Gr' and Bo' have many parameters in common, thus, they could not be manipulated independently. Between Gr' and Bo' it was revealed that Bo' is more important to have similarity of the temperature field [10]. Therefore, Bo' was selected as a similarity parameter, and similarity would be discussed in terms of the Bo'.

$$\frac{\partial u_i^*}{\partial x_i^*} = 0 \tag{4}$$

$$\frac{\partial u_i^*}{\partial t^*} + u_j^* \frac{\partial u_i^*}{\partial x_j^*} = \frac{1}{Gr'^{1/2}} \frac{\partial^2 u_i^*}{\partial x_j^{*2}} - \frac{\beta g \Delta T_{ref} L_{h-c}}{u_{ref}^2} T^* \delta_{i3} - \frac{\Delta P}{\rho u_0^2} \frac{\partial P^*}{\partial x_i^*} \tag{5}$$

$$\frac{\partial T^*}{\partial t^*} + u_j^* \frac{\partial T^*}{\partial x_j^*} = \frac{1}{Bo'^{1/2}} \frac{\partial^2 T^*}{\partial x_j^{*2}} + \frac{Q_0 L}{\rho c_p u_{ref} \Delta T_{ref}} - \frac{Q''}{\rho c_p u_{ref} \Delta T_{ref}} \tag{6}$$

$$Gr' = \left(\frac{\beta g}{\rho c_p}\right)^{2/3} \frac{L^{4/3} Q^{2/3}}{\nu^2} \tag{7}$$

$$Bo' = \left(\frac{\beta g}{\rho c_p}\right)^{2/3} \frac{L^{4/3} Q^{2/3}}{\alpha^2} \tag{8}$$

To simulate the sodium by the Wood's metal, length scale difference is 14 : 25, approximately 1 : 1.8. It means that Wood's metal system should be 1.8 times smaller than the sodium system. However, in the many experimental facility, the scale was compromised as four times different size than required length scale [9,11–13]. By the compromise, Bo' would be slightly distorted, however, many advantages like detailed geometry, easy handling and cost issue could be achieved. Therefore, in our facility, scale was considered up to 1 : 5 in the design integration and summary section.

2.4. Ex-vessel similarity law

For ex-vessel, Ishii's similarity law was employed [27], which was already used in previous scale-downed experiment [21–23]. There are non-dimensionalized form of the energy momentum and energy equation for the fluid, and energy equation for the solid in equation (9) – (11). Important non-dimensional numbers were derived: Richardson number (Ri), friction number (F), and Stanton number (St). Ri represents the ratio of buoyant potential to the inertial force in the natural circulation. Friction number is a summation of the major and minor loss, which are related to the pressure drop similarity of the system. However, it was not considered in the present study because air flow path was quite simplified from the prototype. St is related to the similarity in the heat transfer in terms of the HTC. Because natural circulation heat transfer would be analyzed, Ri and St were selected as key non-dimensional numbers for the ex-vessel similarity like previous works [21–23]. Solid related similarity parameters like the Biot number and heat source number were neglected because of insulation issue and negligible thermal inertia of the RV wall, compared to the whole system.

$$\frac{du_{ref}^*}{dt^*}\left(\sum_l \frac{L_l}{A_l^{*2}}\right) = Ri(T_h^* - T_c^*)L_{heater} - \frac{u_{ref}^{*2}}{2}\left(\sum_l F_l \frac{1}{A_l^{*2}}\right) \tag{9}$$

$$\frac{\partial T_l^*}{\partial t^*} + \frac{u_{ref}^*}{A_l} \frac{\partial T_l^*}{\partial x_3} = St_l\left(T_{s,l}^* - T_l^*\right) \tag{10}$$

$$\frac{\partial T_{s,l}^*}{\partial t^*} + T^* \nabla_l^{*2} T_{s,l}^* - \left(\frac{Q_S L_{heater}}{\rho_s c_{p,s} u_{ref} \Delta T_{ref}}\right)_i = 0 \tag{11}$$

$$Ri = \frac{g\beta \Delta T_{ref} L_{h-c}}{u_{ref}^2} \tag{12}$$

$$F_l = \left(\frac{fL}{D} + K\right) \tag{13}$$

$$St_i = \left(\frac{4hL}{\rho c_p u_{ref} d}\right) \tag{14}$$

There is the length term in the numerator of the Ri. while the St has the length scale term in the numerator, and channel width is in the denominator. In addition, HTC in the numerator of St decreases as the scale decreases in general. Therefore, to keep the Ri as constant with changing scale, if the experimental facility becomes smaller, the velocity should be decreased as a square root of the scale change. In case of the St, it also decreases as the facility becomes smaller. However, there is channel width term d in the numerator of the St, it could be changed independent to the change of the length scale. Detailed similarity was considered based on these concepts.

To evaluate a convective HTC in the numerator of the St, flow was assumed as external flow. Characteristics of the flow in the prototype and model were summarized in Fig. 4 and Table 3. In the PGSFR, because the cross section of the flow channel is a thin ring, it could be represented as flow heated by two opposite infinite walls like (a) in Fig. 4. It was simplified in the SINCRO-IT as single wall heated flow in the rectangular channel. Different to original two

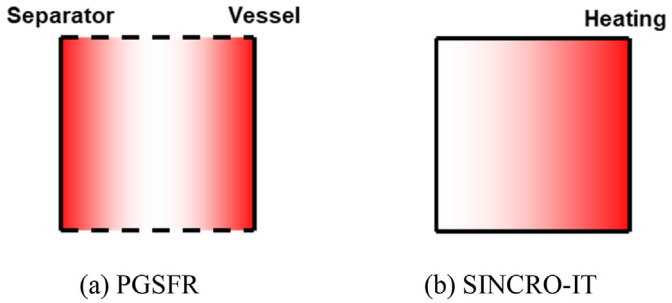

Fig. 4. Schematic of flow boundary condition in the air channel.

opposite walls heating, it was assumed as external flow with the single wall heating. Finally, analytical solution of the external flow HTC was applied for the evaluation of the HTC, like an equation (15).

2.5. Design integration and summary

Based on the similarities for in- and ex-vessel, and matching of the time scales, final scale of the facility was compared in case of 1–3, 4, and 5 scale reduction. Brief specifications and similarities were summarized in Table 4. The specifications of the PGSFR were based on the report published in 2015. Height of the rising channel was 6.7 m in PGSFR, and it was reduced according to the scaling ratio. Gap was increased from original 0.3 m–0.4 m to guarantees the St similarity. Heat flux was 14.5 kW/m^2 in the prototype at the maximum heat removal rate of the RVACS [25], and reduced to the 1 kW/m^2, to make identical time scale for in- and ex-vessel. In– and ex-vessel time scales showed good accordance regardless to the scale. Therefore, mass of the Wood's metal and anticipated temperature difference between the air inlet and outlet were important parameters. The Wood's metal mass was related to the cost of the facility, while temperature difference of the air was related to the data resolution. The Wood's metal mass increases as third power of the scale, therefore, smaller facility is better. The temperature difference of the air increases slightly as the scale increases, from 16.2 to 19.3°C. Considering approximately 1.5°C of the uncertainty of the thermocouple, change of the temperature difference was negligible. Therefore, it is better to designed as a smaller facility in the aspect of characteristics except for the similarities.

Regard to similarities, Bo' was used for the in-vessel, and Ri and St were used for the ex-vessel. For ideal scaling ratio for the Bo' was 1.8, however, it was compromised as smaller facility. Ri could be matched by changing flow rate, while change of the St was negligible. In terms of the in-vessel similarity, it is better to be designed as a larger facility, while ex-vessel showed always good similarity within the scope. Therefore, a larger facility is better to be designed as a larger facility.

Considering conflicting requirements, final scale was determined as 1 : 4. Mass of the Wood's metal could be handled with good resolution of the temperature data. For in-vessel similarity, Bo' was in the reasonable range, while ex-vessel similarity was perfectly achieved. The most important parameter, time scale, showed good accordance for the in- and ex-vessel, as 1 : 1.68, which makes transient experiment possible.

Table 4
Summary of main design parameters in different scale reduction.

	PGSFR [27].	1 : 5	1 : 4	1 : 3
Length.	6.7 m	1.34 m	1.675 m	2.33 m
Gap.	0.3 m	0.4 m	0.4 m	0.4 m
q".	14500 W/m^2	1000 W/m^2	1000 W/m^2	1000 W/m^2
Power.	0.28 MW (0.7 %)	87 W	134 W	223 W
mWoods' Metal.	-	850 kg	1350 kg	2400 kg
ΔT_{air}	200°C	16.2°C	17.5°C	19.3°C
$Time_{in}$	1	1.55	1.67	1.84
$Time_{out}$	1	1.57	1.69	1.86
Bo'	8.14×10^7	3.59×10^6	7.56×10^6	1.97×10^7
St_FC	0.119	0.112	0.116	0.122
Ri	0.86	0.86	0.86	0.86

Table 5
Summary of uncertainty contributors.

Category	Contributor	Magnitude
Power	Voltage	3.00 %
	Resistance	0.14 %
	Total	6.00 %
Flow rate	Velocity	3.00 %
	Area	0.03 %
	Total	3.00 %
Temperature	Thermocouple	0.40 %
	Compensation wire	1.5 K
	Reference temperature	0.5 K
	I/O interface	0.04 %
	AD conversion	0.02 %
	Total	1.72 K

2.6. Uncertainty analysis

In this study, power was given, and flow rate and temperature were measured. Uncertainties related to these parameters were summarized in Table 5. The power was supplied by DC, controlling voltage with a constant resistance of the heater. Uncertainty by voltage was the random error, with 3.00 % of the magnitude. The other contributor of the power was the resistance, which was the systematic error with 0.14 % of the magnitude. Therefore, Total uncertainty of the power was 6.00 %.To measure air flow, KIMO LV

Table 3
Comparison of flow in the air channel in the prototype and model.

$$\overline{Nu_L} = 0.664 \mathrm{Re}_L^{1/2} \mathrm{Pr}^{1/3} \quad (15)$$

	PGSFR	SINCRO-IT
Characteristics.	Square channel - Two non-slip wall with heating - Two adiabatic slip wall	Square channel - One non-slip wall with heating - One adiabatic non-slip wall - Two adiabatic non-slip wall
q".	14.5 kW/m^2	1 kW/m^2
Re_L	403400 (laminar)	26500 (laminar)
Correlation.	**Analytical,** internal	**Analytical,** internal

110 was used for our flow meter with K 25-85 air flow cone. It was calculated from the velocity, which contains the random error, which has 3.00 % of the reading error. There is only one additional systematic error contributors in the flow rate because flowmeter directly indicates the flow rate without auxiliary systems like data acquisition system. Uncertainty from the area of the flow cone was 0.03 %, and final uncertainty of the flow rate was to 3.00 %. Temperature was measured by the K-type thermocouple, which has 0.4 % of the uncertainty the reading. Uncertainties in the compensation wire and reference temperature were 1.5 K and 0.5 K respectively. System related uncertainties were 0.04 % of input/output interface and 0.02 % of AD conversion. Among these contributors, only reference temperature error was the random error, while the other contributors were the systematic error. Considering all these factors, final uncertainty in the temperature was 1.72 K.

3. Experimental analysis and code validation

Experiments for the RVACS performance evaluation were conducted in the SINCRO-IT facility, and the data were translated to an arbitrary reactor, which has very similar characteristics with prototype PGSFR. Because it was simplified as 2-D, data from the SINCRO-IT could not be directly translated to that of the PGSFR. Therefore, the data were interpreted to the that of a corresponding, arbitrary 2-D reactor. The system code was also based on the arbitrary 2-D reactor.

3.1. Data interpretation from the model to prototype

Final objective of the experiment is to provide data for the system code validation. Therefore, the experimental data, which were obtained by Wood's metal / air experiments, should be interpreted to the data of the original system with sodium and air. In this part, data interpretation methodology was introduced with an example, 1.0% decay heat of the steady state.

Considering the heat transfer circuit of the RVACS, to obtain the maximum sodium temperature, it should be calculated from the air inlet temperature, which is a kind of boundary condition for the RVACS. The wall temperature is determined by the air temperature, a cooling heat flux, and HTC of the air. The temperature difference between the inner and outer surface of the wall is determined by the heat flux, a thickness and thermal conductivity of the wall. The sodium temperature could be obtained based on the heat flux, HTC of the sodium, and inner wall temperature. Finally, the maximum sodium temperature, which is related to the sodium boiling, could be obtained using temperature distribution in the natural circulation. This procedure is summarized in Fig. 5, and equations were summarized in Table 6.

To calculate maximum sodium temperature, inner wall, and outer wall HTC should be obtained in the experiment. However, there was a problem with measuring exact inner and outer wall temperature for technical issue. Approximately 1.5 tons of the Wood's metal was in the pool, and the wall thickness was only 8 mm. In addition, it was hard to accurately measure the wall surface temperatures, therefore, the thermocouples were omitted. The temperature of the inner and outer surface of the wall were obtained using correlations.

Temperature at the inner surface of the wall was obtained by the based on the general Churchill & Chu correlation, which is summarized in equation (20), using average sodium temperature near the wall and the heat flux. Definitions of the Rayleigh number (Ra) and Prandtl number (Pr) were in the equation (21) and (22). Then, the outer surface temperature could be easily calculated using simple conduction equation (17). The air-wall HTC also could be simply obtained using outer surface temperature of the wall and the air temperature. This air-wall HTC used to check the validity of the evaluation, compared with estimated HTC by various correlations.

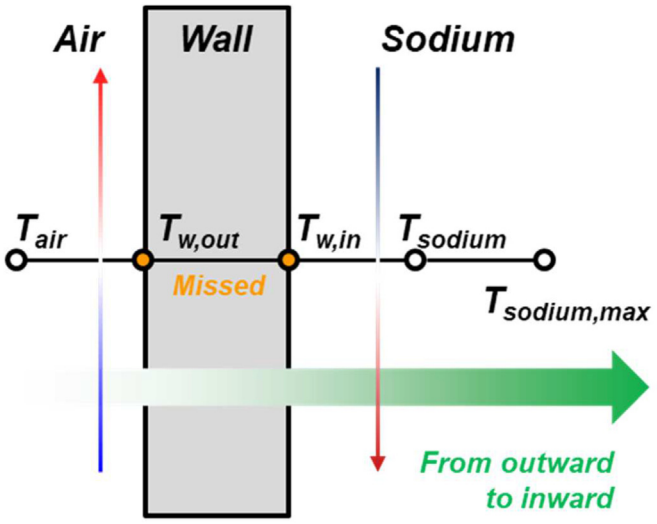

Fig. 5. Schematic of the temperature interpretation.

$$\overline{Nu_L} = 0.68 + \frac{0.67Ra_L^{1/4}}{\left[1 + (0.492/\mathrm{Pr})^{9/16}\right]^{4/9}} \tag{20}$$

$$Ra = Gr_L\mathrm{Pr} = \frac{g\beta(T_s - T_\infty)L^3}{\nu\alpha} \tag{21}$$

$$\mathrm{Pr} = \frac{\nu}{\alpha} \tag{22}$$

Before direct comparison between the experimental air-wall HTC obtained like above, and an anticipated HTC by correlations, the fin effect should be considered. Only one side of the rectangular duct was designed to heat the air, which is contact to the Wood's metal pool, like (a) in Fig. 6. However, insulation between the heating wall and the other walls was failed due to technical issues. Therefore, the channel was heated with fin effect the adjacent wall, like (b). The fin effect could be treated as a multiplication of the HTC coefficient, and an HTC after correction were compared.

Table 7 shows calculation process and results of the fin effect. The axial height of the fin was equal to the height of the fin, 1.675 m. The fin thickness was same to the that of the duct wall, 0.005 m. The fin was treated as an infinite fin because it satisfied mL > 2.65. Equations for fin calculation were summarized in equation (23) – (26). Finally, considering fin effectiveness, overall surface effectiveness was 3.20, and a corrected convective HTC was 6.71 W/m^2.K. It was in the range of the general air convective HTC, 4–20 W/m^2.K, thus, it was properly corrected (see Table 8).

$$m_{fin} = \sqrt{\frac{hP}{kA_c}} \tag{23}$$

$$q_{fin} = M = \sqrt{hPkA_c\theta_b} \tag{24}$$

Table 6
Summary of the equations for temperature calculation.

Part	Equation	Notes
Air convection at wall	$q'' = h_{air}\Delta T_{air-wall}$ (16)	h_{air} was simulated
Wall conduction	$q'' = \frac{k_{wall}}{d_{wall}}\Delta T_{wall\ in-out}$ (17)	$T_{wall,in}$ and $T_{wall,out}$ were estimated
Pool convection at wall	$q'' = h_{sodium}\Delta T_{sodium-wall}$ (18)	H_{sodium} was estimated
Pool natural circulation	$\Delta T_{sodium} = \frac{\Delta T_{ref,sodium}}{\Delta T_{ref,Wood's\ metal}}\Delta T_{Wood's\ metal}$ (19)	ΔT was simulated

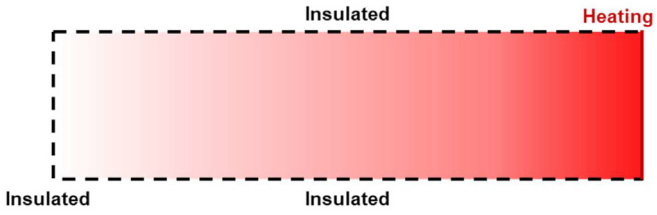

(a) Ideal case – insulated heating surface

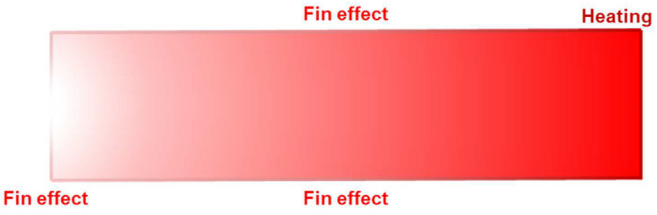

(b) Practical case – fin effect through attached wall

Fig. 6. Schematic of the fin effect at the duct cross section.

Table 7
Summary of the fin effect.

Parameter	Value	Notes
Axial height	1.675 m	Channel height
Fin thickness	0.005 m	Same to duct thickness
Boundary condition	Infinite	mL = 4.10 > 2.65
Heat transfer area	0.1843 m^2	
Base area	0.008375 m^2	
Fin thermal conductivity	16.2 W/m.K	Stainless steel
Fin effectiveness	21.94	Regard to base area
Overall effectiveness	3.20	Regard to whole area
HTC after correction	6.71 W/m^2.K	4–20 W/m^2.K in general

$$\varepsilon_{fin} = \frac{R_{t,b}}{R_{t,f}} = \sqrt{\frac{kP}{hA_c}} \tag{25}$$

$$\varepsilon_{surface} = \frac{\left(w_{duct} - 2w_{fin}\right) + 2w_{fin}\varepsilon_{fin}}{\left(w_{duct} - 2w_{fin}\right)} \tag{26}$$

To validate the corrected HTC, it was compared to the HTCs by various correlations. Because operation condition of the SINCRO-IT included some ambiguousness, correlations for various flow regimes like forced and natural convection, and laminar and turbulent flow were considered. As an internal flow, analytical solution and general Dittus-Boelter equation were considered. Because anticipated HTCs were far below the experimental HTC, an external flow assumption looked more reasonable than assuming as an internal flow. With the external flow assumption, analytical solutions and Churchill & Chu correlations were considered. Depending on the length selection for the Nusselt number calculation, the HTC was 5.91 and 8.69 W/m^2.K, while the corrected experimental HTC was 6.71 W/m^2.K. Therefore, the corrected experimental HTC was in reasonable range, and the validity of the fin analysis and the HTC calculation were proven.

Overall data interpretation process is summarized in Table 9. Conversion ratio of the heat flux was 14.5, which was obtained by the Ishii's law. Schematic of the temperature interpretation was summarized in Fig. 5, and through aforementioned assumptions, temperature of the prototype was calculated. It started from the air inlet temperature, which is given by the environment. Therefore, temperature of the air inlet of the prototype was same to that of the experiment. Air outlet temperature could be calculated by the temperature difference conversion ratio by Ishii's law, and air average temperature was 85.1°C for the prototype. Temperature difference between the wall and air was calculated using the HTC with conversion ratio and heat flux with conversion ratio. Wall external temperature 719.2°C, while internal temperature was 733.4°C, which could be obtained with simple conduction equation. The HTC of the pool natural circulation was 2.28 times larger in the prototype than the experiment, so that pool temperature near the wall was 745.5°C for the prototype. Temperature difference in the pool between the region near the wall and the maximum pool

Table 8
Comparison of air heat transfer coefficient.

Condition		HTC [W/m^2.K]	Equation	Notes
Internal	For.-Lam.	0.58	$Nu = 3.66$ (27)	
	For.-Tur.	2.11	$\overline{Nu_D} = 0.023\mathrm{Re}_D^{0.8}\mathrm{Pr}^{0.4}$ (28)	
External	For.-Lam.	1.70	$\overline{Nu_L} = 0.664\mathrm{Re}_L^{1/2}\mathrm{Pr}^{1/3}$ (29)	
		2.17	$\overline{Nu_L} = (0.037\mathrm{Re}_L^{4/5} - 871)\mathrm{Pr}^{1/3}$ (30)	Entrance effect
	Nat.-Tur.	5.91		L_{heater}
		8.69	$\overline{Nu_L} = \left[0.825 + \frac{0.387Ra_L^{1/6}}{\{1+(0.492/\mathrm{Pr})^{9/16}\}^{4/9}}\right]^2$ (31)	$L_{heater\ +\ chimney}$

Table 9
Data interpretation from the experiment to the prototype.

Position	Experimental value	Conversion parameter	Conversion ratio	Interpreted value	Notes
Air inlet	10.1°C			10.1°C	Reference point
$\Delta T_{air\ in\text{-}out}$	13.2°C	ΔT	11.43	150.0°C	Ishii's law
Air outlet	23.3°C			160.1°C	Experimental
Air average	16.7°C			85.1°C	
	21.4 W/m^2.K	HTC	1.30	27.9 W/m^2.K	Ishii's law
Wall, out	73.5°C			719.2°C	
Wall, in	74.4°C			733.4°C	Ishii's law
	637.9 W/m^2.K	HTC	2.28	1456.7 W/m^2.K	Ishii's law
$Pool_{wall,\ average}$	76.3°C			745.5°C	
$\Delta Pool_{N.C.}$	6.4°C	ΔT	0.92	5.9°C	Bo' based law
Pool max.	82.7°C			751.4°C	

temperature could be obtained employing Bo' based law. Temperature difference in the natural circulation field was 5.9°C for the prototype. Therefore, the maximum sodium temperature could be predicted as 751.4°C.

3.2. Test matrix

The overall RVACS performance is better to be analyzed with system codes because of large scale and neutronic feedback. Therefore, the SINCRO-IT experiments should provide validation data for the RVACS module in system codes. Both steady and transient experiments were planned. In the steady state experiments, overall system temperature at certain decay heat was obtained. In actual situations, the decay heat, thermal inertia of the system, change of the air flow rate and corresponding RVACS performance are continuously changing, therefore, there is no steady state in the actual situation in the strict sense. Nevertheless, they were conducted to suggest the maximum RVACS heat removal rate without violation of the safety limits in the aspects of the long-term cooling, which could be assumed as a quasi-steady state. Although the geometry was simplified from 3-D to 2-D, main safety parameters would be compared with previous articles. Final test matrix for the steady state were summarized in Table 10. Power in the SINCRO-IT corresponding to the decay heat was 1395.5 W in case of the 1.0 % of the decay heat. Air flow rate was fixed as 44.5 m^3/h, which corresponds to the maximum air flow rate of the RVACS [45].

Regard to the transient experiments, it was the best to simulate design basis accidents. For the PGSFR, there are loss of flow (LOF), transient over-power (TOP), station black out (SBO), and loss of heat sink (LOHS) [6,25]. However, these scenarios could not be reproduced in the SINCRO-IT. There scenarios could be generalized by the reactor trip signal and following reactor trip, primary pump coastdown, IHX isolation, and the RVACS damper opening also known as the RVACS activation. Since all these scenarios are started from the normal operation, IHX operation and pump are required to simulate initial condition of the scenario. However, there is no pump in the SINCRO-IT, and applied similarity law cannot guarantee the similarity under forced operation. Therefore, the accident scenario was selected as an arbitrary re-criticality after safe shutdown, which have no relationship with the pump. Initial and changed power were determined to have proper temperature range for evaluating sodium boiling. By these arbitrary scenarios, temperature increase of the system, development of the coolability could be analyzed.

Initial state of the transient experiments was started from the steady state approximately 1.0 % of the decay heat. Power increase after re-criticality was assumed as sudden increase and maintenance like the step function. 2.0 % and 10.0 % of the power were assumed after re-criticality, which are enough to predict the sodium boiling (See Table 11).

Table 10
Test matrix for the steady cases.

Decay heat	Time after shutdown	Air flow rate	Notes
0.6 %	56.5 h	44.5 m^3/h	
0.7 %	49.2 h		Max. heat removal [25].
0.8 %	42.9 h		
0.9 %	37.3 h		
1.0 %	32.3 h		Heat balance test
1.1 %	27.8 h		
1.2 %	23.6 h		
1.3 %	19.7 h		Sodium boiling predicted

3.3. Nodalization of the system code

Using the experimental data obtained with the SINCRO-IT, a capability of a system code on simulating the natural circulation inside the pool and heat transfer through the air-cooling channel (which reflects RVACS of the PGSFR), was identified. In this paper, the TRACE code was used. The TRACE code is a neutronic-thermal-hydraulic analysis code developed by the U.S.NRC, which has been widely used in the field of nuclear engineering.

The nodalization of the SINCRO-IT for the TRACE code was developed using a SNAP program, which provides graphical user interface for generating an input deck. A VESSEL component was used to simulate the pool containing sodium. The VESSEL component is a 3-dimensional component which can be discretized in x-direction, y-direction and axial direction. The VESSEL was divided in 10 nodes in width-direction and 17 nodes in axial level. Note that VESSEL was not divided in depth-direction, as the behavior of sodium in depth-direction was not the major issue. The core of the SINCRO-IT was placed from 8th node to 10th node in width-direction and 3rd to 4th node in axial direction. The core was reflected into the model by using the fluid power option, which provide a volumetric heat source for the specified region.

Partitions, which divide the pool and guide the natural circulation flow (orange wall in Fig. 7), was modeled by adjusting the flow area between cells of the VESSEL. Above the VESSEL component, a single-volume PIPE component and a BREAK component were placed to maintain the pressure stably. The HX for normal operation (blue system in Fig. 7) was modeled using a heat structure with constant temperature.

The air-cooling channel was modeled using a PIPE, a FILL and a BREAK component. FILL simulated the inlet of the external air-cooling channel, while the BREAK served as an outlet. Here, the radiation heat transfer was neglected. Two heat structures were used to model the heat transfer between pool and air-cooling channel, so that convective heat transfer (occurred on the wall) and conductive heat transfer (transfer heat from pool to air-cooling channel) were modeled. The heat transfer area of the heat structure

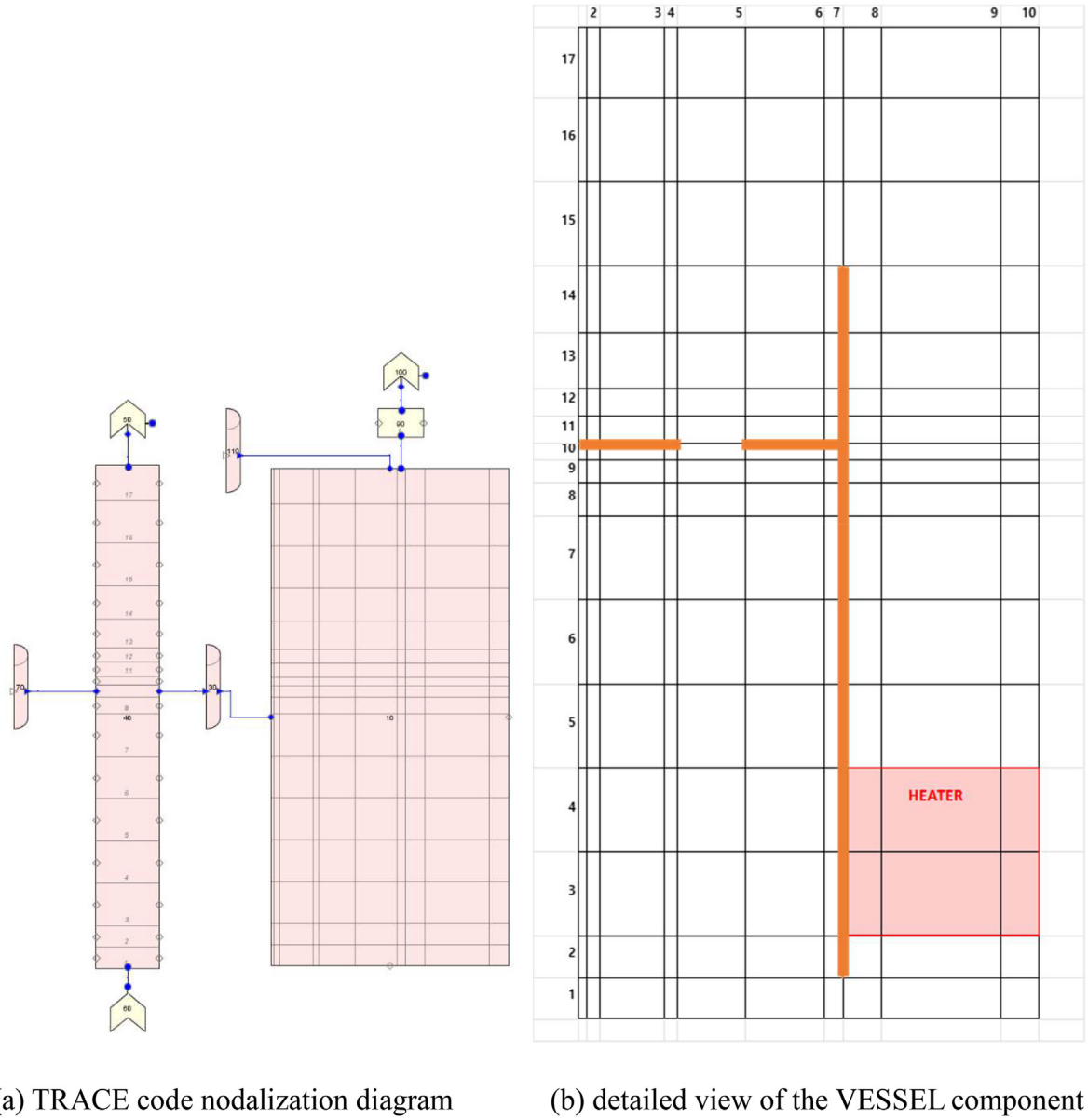

Fig. 7. TRACE code nodalization diagram.

was adjusted to incorporate the effect of fin, which is shown in Fig. 6. The nodalization diagram is shown in Fig. 7.

3.4. Heat balance test

Heat balance was tested in two conditions: 1.0 % and 2.5 % of the decay heat. Since the facility was designed to remove heat only through air cooling channel, the insulation rate was defined as the ratio of the heat removed via the air cooling to the heat input by the cartridge heaters. The heat removal via air cooling was calculated based on the inlet and outlet temperature of the air like equation (32). As written in the uncertainty analysis, total uncertainty in the flow rate was 3.00 %. Uncertainty in the temperature difference between the inlet and outlet could be summarized like equation (33). The uncertainty of the thermocouple was 1.72 K. According to the calculation, uncertainty in the temperature difference was 1.68 and 3.65 %, depending on the test conditions, because the temperature was determined based on the average of recent 10 moments. Considering both uncertainty of flow rate and temperature, final error of the heat output of the heat balance test was 3.43, and 4.73 %.

$$Q_{air-cooling} = \dot{m} c_{p,air} \Delta T_{air,in-out} \tag{32}$$

$$U_{\Delta T_{in-out}} = \sqrt{\left(\frac{\partial \Delta T_{in-out}}{\partial T_{in}} \times U_{T_{in}}\right)^2 + \left(\frac{\partial \Delta T_{in-out}}{\partial T_{out}} \times U_{T_{out}}\right)^2} \tag{33}$$

The results were summarized in Table 12. It was tested in the 2.5

Table 11
Test matrix for the transient cases.

Initial power (steady)	Changed power	Air flow rate
1.0 % 1.1 %	2.0 % 10.0 %	44.5 m^3/h

Table 12
Summary of the heat balance test.

Condition	Parameter	Value
High temperature	Power	534 W (2.5 %)
	Heat flux	3191 W/m^2
	Air flow rate	46.5 m^3/h
	$\Delta T_{theoretical}$	32.4°C
	$\Delta T_{experimental}$	29.2°C
	Insulation rate	90.1 %
Low temperature	Power	236 W (1.0 %)
	Heat flux	1409 W/m^2
	Air flow rate	44.5 m^3/h
	$\Delta T_{theoretical}$	14.9°C
	$\Delta T_{experimental}$	13.1°C
	Insulation rate	87.6 %

% and 1.0 % of power, which could be categorized as high temperature and low temperature, respectively. Heat was designed to be removed only RVACS air channel. In case of high temperature condition, temperature of the Wood's metal was approximately 140°C, with approximately 3200 W/m^2 of the heat flux. Air flow rate in the channel was 46.5 m^3/h, which corresponds to 0.016 kg/s and 0.32 m/s. In case of perfect insulation, temperature difference between the air inlet and outlet would be 32.4°C, while it was 29.2°C in the test. Therefore, the insulation rate was obtained as 90.1 %. In case of low temperature condition, temperature in the perfect insulation was 14.9°C, while 13.1°C was observed in the test. The insulation rate was 87.6 % in the low temperature case. As a result of the heat balance test, both conditions showed satisfactory insulation performance. Following experiments were analyzed based on the well-insulated facility.

3.5. Steady state experiments

Considering data interpretation process, error contributors of the interpreted temperature were heat flux and temperature. However, uncertainty from the heat flux evaluation was neglected and heat flux was assumed as true. The heat flux was calculated using the power from equation (32) and area. In case of the steady state, random error from the temperature difference could be mitigated by measuring multiple samples, like in heat balance tests. However, in case of the transient case, the temperature difference could be measured at only once. If the temperature difference measured just one time, the uncertainty was evaluated as 15.50–18.95 %. It was an error enough to make discussion on the interpreted data meaningless. Therefore, the error contribution from the heat flux was not considered and only temperature error took into consideration. For the temperature, there are three uncertainty contributors during the data interpretation: average air temperature, and ΔT between average air temperature and the pool, and ΔT in the pool. Uncertainty from the average air temperature and T in the pool are simple. However, a conversion ratio of the temperature difference between average air and pool near the wall was not clear. As written in section 3.1, there were many temperature points were missed and they were estimated from correlations. Regard to the estimated temperature difference, overall conversion ratio was calculated by equation (34). Each temperature difference was multiplied by the heat flux ratio and divided by the HTC conversion ratio considering its proportion. Therefore, overall conversion ratio was 11.06, and it was very similar to $\Delta T_{air\ average\text{-}wall}$ (14.5/1.3 = 11.15), which was the major ΔT. Overall process were summarized in Table 13.

$$Overall\ conversion\ ratio_{\Delta T} = \sum_i \frac{\Delta T_i}{\Delta T_{total}} \times \frac{Heat\ flux\ multiplication_i}{HTC\ conversion\ ratio_i} \quad (34)$$

From the overall conversion ratio between the air and the pool, temperature uncertainties during data interpretation were summarized in equation (35). As shown in the equation, the final interpreted pool temperature could be expressed a combination of the experimental temperatures. By combination of the uncertainty of each temperature and coefficients in each term in equation (35), final uncertainty of the pool temperature could be obtained, like Table 14. Uncertainty from the pool temperature was divided by $8^{1/2}$ because it was the average of the 8 points.

For steady state cases, it was tested from 0.6 % to 1.3 %, with 0.1 % of increment. Fig. 8 (a) shows representative temperature distribution of the SINCRO-IT at 1.0 % of the decay heat. Most of the scenarios include IHX isolation and pump coastdown after reactor shutdown. Then, RVACS was activated. As described in the design, the SINCRO-IT facility had no other decay heat removal systems, and only RVACS was into the design. Therefore, the effect of the RVACS could be observed solely. Overall, the temperature distribution was stratified. Above the heater, the Wood's metal was heated approximately 81–82°C, to the upper plenum. The maximum temperature was observed in the upper plenum, which was 82.7°C. Heated Wood's metal flowed to the cooling boundary, which was represented by a blue vertical line on left-hand side in the figure. Although there was the heat exchanger on the left-side of the upper plenum, the temperature did not change because it was isolated. Temperature near the cooling boundary showed always slightly lower temperature than the adjacent regions, therefore, it could be concluded that heat was removed by the cooling boundary. The redan, which separates upper and lower plenum in the prototype, was reflected into the SINCRO-IT as a horizonal partition. Through the hole in the horizontal partition below the heat exchanger, the Wood's metal came down. In the lower plenum, it was common that temperature near the wall was lower than adjacent points. In Fig. 8 (a), there was a solidified region in the left side of the bottom. The freezing point of the Wood's metal is 73–77°C, depending on literatures, thus, there could be solidification below approximately 75°C. Because air entered from the bottom and Wood's metal flowed to the top, temperature of the pool bottom was the lowest, even below the freezing point of the Wood's metal. The pool was cooled by the direct contact with the cooling boundary and through the solidification region, to approximately 79°C. It re-entered and rose to the heating region, right after the separator. In the core region, because of the suction by upward flow at the heating zone, the upward flow was started from the right after the separator, and reached to the heating zone. Because of the transverse momentum generated between the separator and the heating zone, natural circulation flow rose along the right wall of the pool, and it could be observed by the temperature distribution at the upper plenum. There was an additional point lower than the freezing point, the lowest point of the right side of the pool. Considering the flow near the heating zone, which rose right after the separator, the lowest point of the right side was excluded from the natural circulation. Although there was no significant cooling through the right side and down side of the pool, this region was cooled enough to solidified.

Fig. 8 (b) was translated into the data of the prototype, according to the discussion on 3.1. The natural circulation characteristics were maintained the same after the data interpretation. Since the heat flux was increased 14.5 times by the similarity law, overall temperature difference in the system was increased, especially for the

Table 13
Derivation of the overall conversion ratio.

$$T_{pool} = T_{air,in} + CR_{air}\frac{1}{2}\Delta T_{air,in-out} + CR_{air-pool}\Delta T_{air-pool} + CR_{pool}\Delta T_{pool} = T_{air,in} + 11.43\frac{1}{2}(T_{air,out} - T_{air,in}) + 11.06\left[T_{pool,near\ wall} - \frac{1}{2}(T_{air,out} + T_{air,in})\right] + 0.92\left[T_{pool} - T_{pool,near\ wall}\right] = -10.245T_{air,in} + 0.185T_{air,out} + 10.14T_{pool,near\ wall} + 0.92T_{pool} \quad (35)$$

	Value	HTC conversion ratio	Heat flux multiplication
$\Delta T_{air\ average\text{-}wall}$	57.06 K	1.3	14.5
$\Delta T_{wall\ inside}$	1.05 K	1	14.5
$\Delta T_{wall\text{-}pool}$	1.93 K	2.28	14.5
ΔT in the experiment.	60.04 K	11.06 times	
ΔT after data interpretation.	663.85 K		

Table 14
Uncertainty analysis in the translated data.

Point	Uncertainty in the experiment	Coefficient	Magnitude
Air inlet	1.72 K	-10.245	-17.62 K
Air outlet	1.72 K	0.185	0.1 K
Pool, near the wall	1.72 K / $8^{1/2}$	10.14	6.17 K
Pool	1.72 K	0.92	1.58 K
Total			**18.74 K**

air inlet and outlet, and the wall and air. Regard to the temperature difference between the air and wall, it was overestimated because only convection was considered in the experiments. Temperature difference inside of the pool was decreased. Due to the limits of the interpretation methodology, the solidification phenomena were not considered. Temperature of the solidified regions were slightly underestimated, however, its effect on the maximum temperature of the sodium could be negligible.

The results of parametric study on the decay heat were summarized in Table 15. Without radiation heat transfer, temperature limit for the RV was 650°C, while sodium boiling limit was approximately 900°C. There was no significant trend change whether there was Wood's metal freezing or not. Therefore, the effect of the solidification of the simulant on the final translate data could be neglected. Regard to the RV temperature, the limit was violated approximately 0.8 % of the decay heat. For the sodium boiling, it was predicted at approximately 1.3 % of the decay heat. Therefore, in this geometry, safety margin for the RV creep was less than that of the sodium boiling. However, these data could not be directly applied to the PGSFR because the radiation heat transfer was neglected. Due to limitation of the simulating experiment, high temperature and corresponding radiation heat transfer was neglected and only convection was considered during the design. In addition, the SINCRO-IT was greatly simplified. Simplification of the pool geometry reduced flow resistance of the natural circulation flow inside of the RV, therefore, difference between the maximum pool temperature and wall temperature was also reduced. These data could be used for the validation of the system code with the simplified geometry. It is reasonable to calculate the PGSFR status based on the validated system code.

The results of the TRACE code benchmarking on SINCRO-IT test are shown in Fig. 9. To simulate experiment, the radiation heat

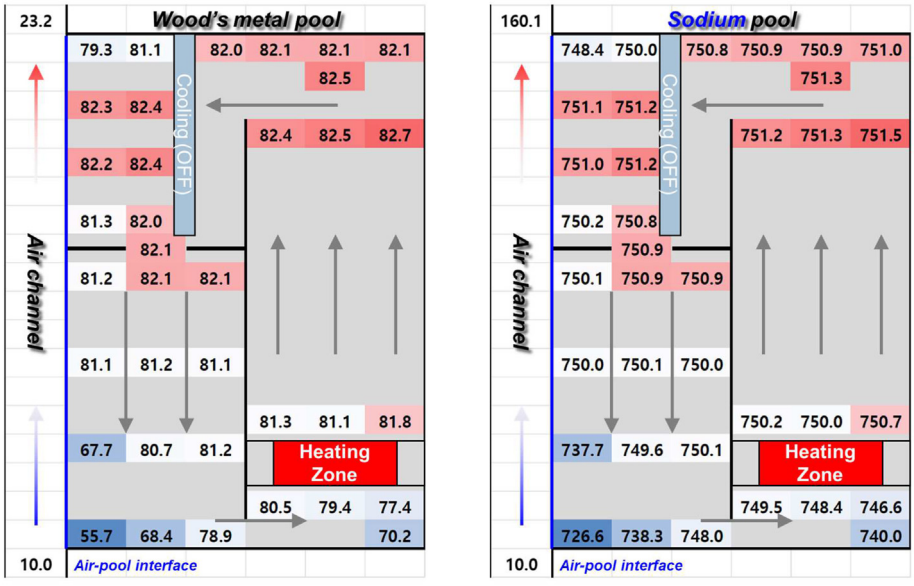

(a) in SINCRO-IT (b) interpreted

Fig. 8. Representative result of the steady state – 1.0 %.

Table 15
Summary of the steady state results.

Power	$T_{air,\ inlet}$ [°C]	RV temperature [°C]		Sodium max temperature [°C]	
		Experimental	Interpreted	Experimental	Interpreted
0.64 %	13.7	65.9	505.6	75.1	528.5
0.68 %	8.2	54.7	531.6	73.7	555.9
0.83 %	10.2	70.2	667.6	81.6	689.2
0.96 %	5.7	64.1	706.0	80.5	726.6
1.01 %	10.1	74.4	733.3	82.7	751.3
1.13 %	6.3	81.5	829.1	85.1	846.6
1.20 %	10.2	86.3	864.7	91.1	882.1
1.33 %	10.5	92.5	931.8	96.8	950.2

transfer option was deactivated. Two different power conditions, 0.68% and 0.96% cases, were served as a data for benchmark. The results were shown as a ratio of predicted temperature using TRACE to the experimental value. It can be recognized that the TRACE code simulated the temperature field inside the pool very accurately; the average ratio of temperature between the experiment and simulation result was about 0.97 in 0.68% case and 0.96 in 0.96% case. The TRACE code also precisely simulated the temperature field; the variance of the temperature ratio was no larger than 0.03 in most of the temperature field.

The natural circulation flow inside the pool due to the sodium heating and cooling at heating zone and wall adjacent to the cooling channel was simulated reasonably. The temperature increment across the heating zone in TRACE code simulation support this. In Fig. 9, the temperature difference across the heating zone was almost same in the TRACE code simulation, and the temperature ratio at the inlet and outlet of the heating zone were very consistent. The thermal stratification, which was observed in the SINCRO-IT experiment, was also observed in the TRACE code simulation. The temperature of the upper plenum tended to be higher than the temperature of the lower plenum.

Meanwhile, the ratio of air cooling channel outlet temperature was about 1.0 and 0.91 in 0.68% and 0.96% cases respectively. The difference of the air cooling channel outlet temperature was due to the heat loss of the experiment, which was explained in Section 3.4. Through the comparison with the experimental data, it was concluded that the TRACE code was capable to predict the temperature field in steady-state, and also capable to predict the heat removal rate to the air cooling channel.

3.6. Transient experiments

In the transient experiments, temperature change along the pool was important, therefore, temperatures of each region were represented as an average of the region, like Fig. 10. Temperature distribution was represented as core inlet, outlet, heat exchanger side, heat exchanger outlet, lower plenum, and bottom of the pool. Temperature of the upper plenum was represented by heat exchanger side near the cooling wall, and heat exchanger outlet, which is the passage the upper and lower plenum.

Heat balance during the transient was discussed with the experimental data, like Fig. 11. The objective of the experiment was to predict sodium boiling, therefore, it was stopped before new equilibrium. In case of 1.0 → 2.0 %, at the steady state before transient, heat input was 225 W, while 200 W of the heat was removed through the RVACS. It corresponds to the insulation rate in the previous discussion. Heat input was increased to 466 W, as the step function, while heat removal through the RVACS was gradually

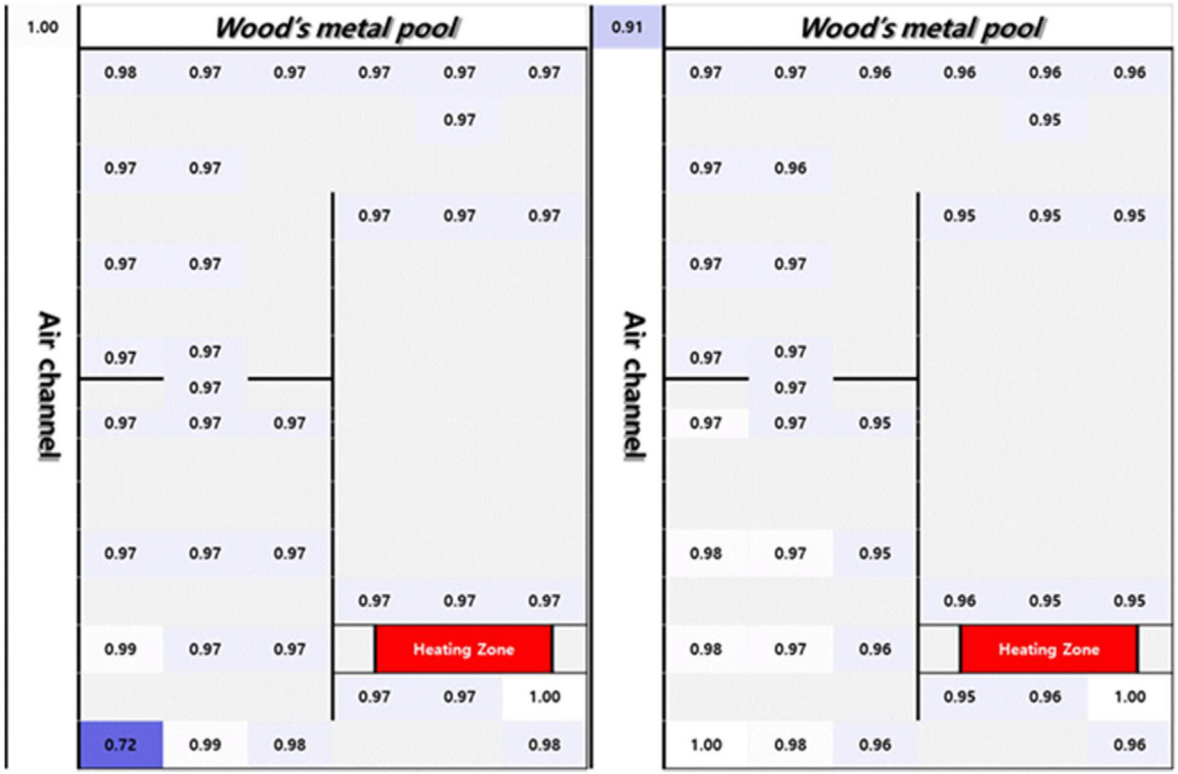

(a) 0.68% case (b) 0.96% case

Fig. 9. Steady-state experiment benchmark results: ratio of predicted temperature to experimental temperature.

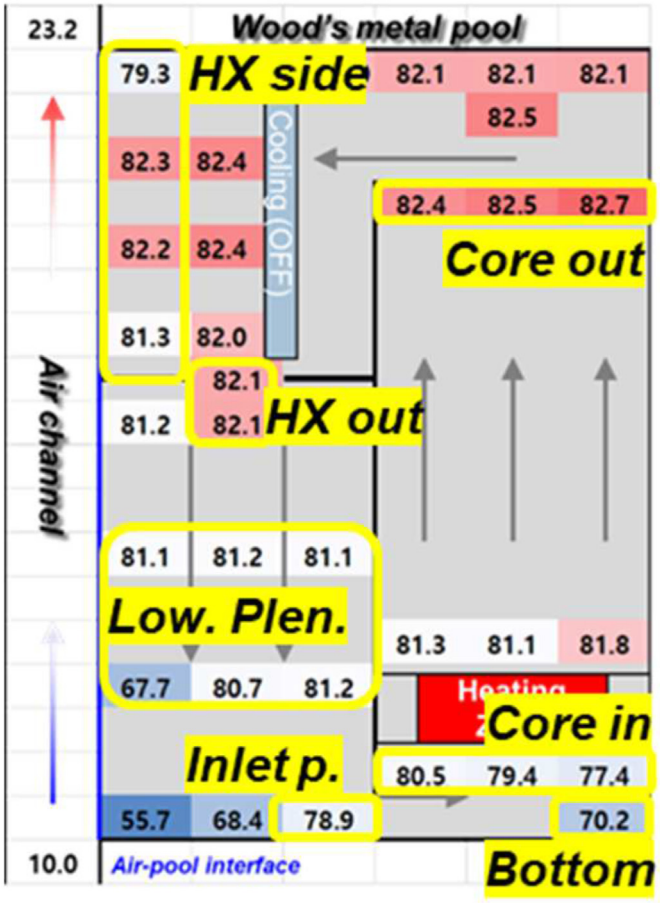

Fig. 10. A legend for transient experiments.

increased. After 84,000 s, the performance of the RVACS was continuously developed, however, it only reached to 330 W, which was 71 % of the increased heat input. Considering heat insulation rate, the new equilibrium state at the increase power was not achieved even after a day. The experiment was over at 84,000 because the temperature inside of the pool was high enough to predict sodium boiling. The situation was same to 1.1 → 10.0 % case. At the steady state, heat input was approximately 250 W, while 222 W was removed. The experiment was over at 18,000 due to rapid temperature increase. After 18,000 s, heat input was approximately 2,388 W, while only 390 W of the heat was removed through the RVACS. It was only 16 % of the heating. Therefore, it could be concluded that RVACS performance change by the sudden power increase was quite slow due to the large thermal inertia of the system. A new equilibrium state between the heating and cooling after power increase was not observed in the given time during the experiment.

Temperature transient was summarized in Fig. 12. Almost linear temperature increase was observed in the high temperature region like the core in, out and upper plenum. On the other hand, in the lower plenum, inlet piping, and pool bottom, there was delay of the temperature increase. Solidification of the Wood's metal caused the delay of the temperature increase in the first half of the transient. After temperature increase over than the melting point, temperature of the region followed the global increase. Whole pool seemed to be melted at approximately 60,000 s, therefore, global temperature increase was observed in the whole pool. Similar to the steady state discussion, in terms of the overall temperature distribution of the system, the temperature difference between the air and wall was the most significant. Temperature distribution inside of the pool could be less significant than the experiment, thus, the error caused by the solidification of the Wood's metal was mitigated. (b) of the Fig. 12 showed the interpreted data of the transient experiment. By the translated data, the sodium boiled at approximately 25,100 s after transient, which corresponds to approximately 42,200 s in the experiments. The maximum temperature was observed at the core outlet, where showed the highest temperature in the steady state.

In case of 1.1 % → 10.0 % case, which was shown in Fig. 13, overall tendency was basically the same except for the temperature increase rate. Compared to the 1.0 → 2.0 % case with 6.1°C of the inlet temperature, air inlet temperature of the present case was 2.6°C. Therefore, initial temperature did not show significant difference with the previous case, although power was slightly higher. Because the air inlet temperature was lower, more regions were solidified. At the inlet piping, concave temperature increase was observed, which was related to melting, while it was convex in the previous case. However, all these differences could be negligible as

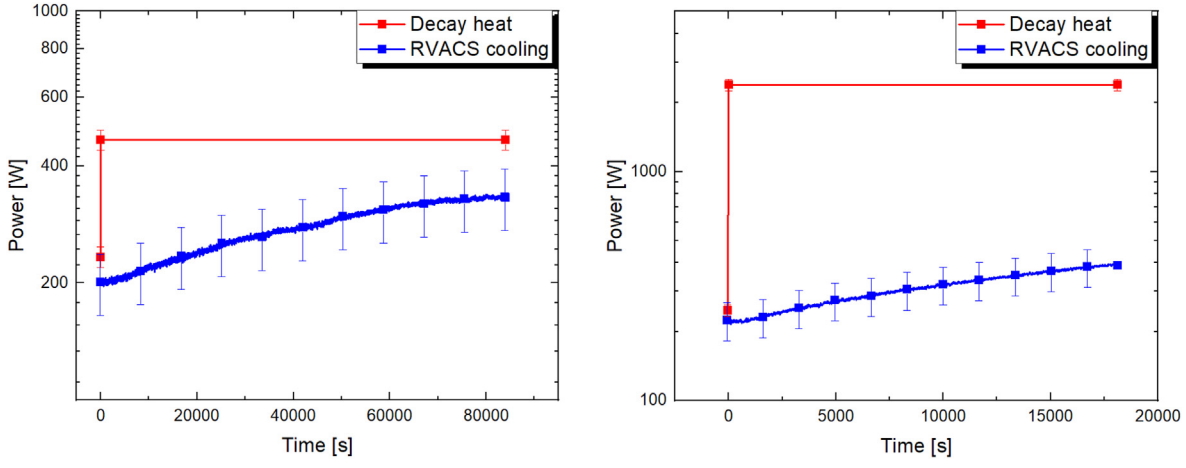

(a) 1.0 → 2.0 %

(b) 1.1 → 10.0 %

Fig. 11. Transient heat balance.

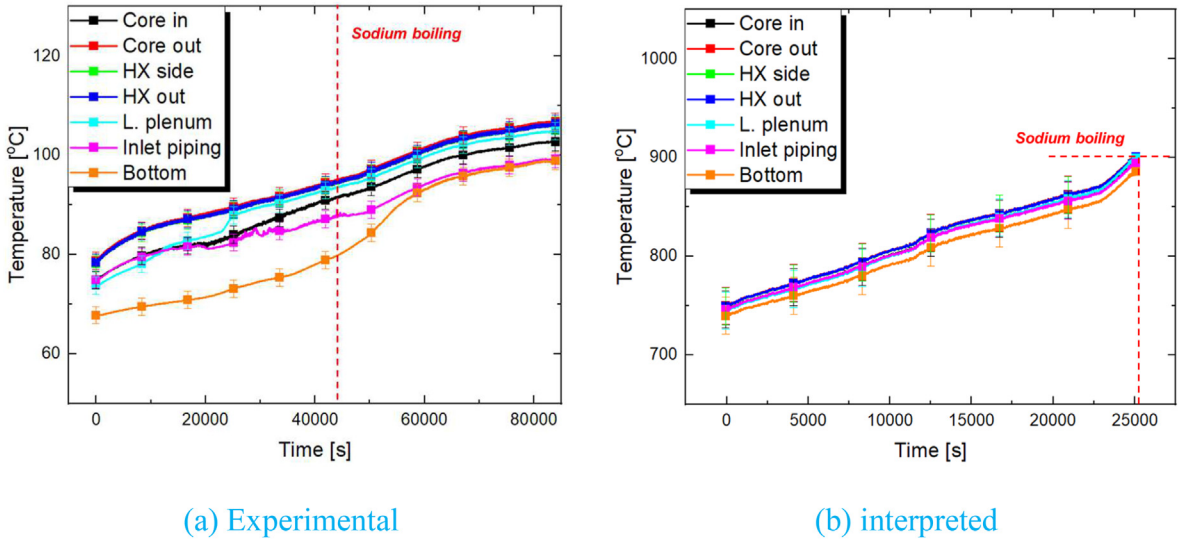

Fig. 12. Transient summary, 1.0 → 2.0 %.

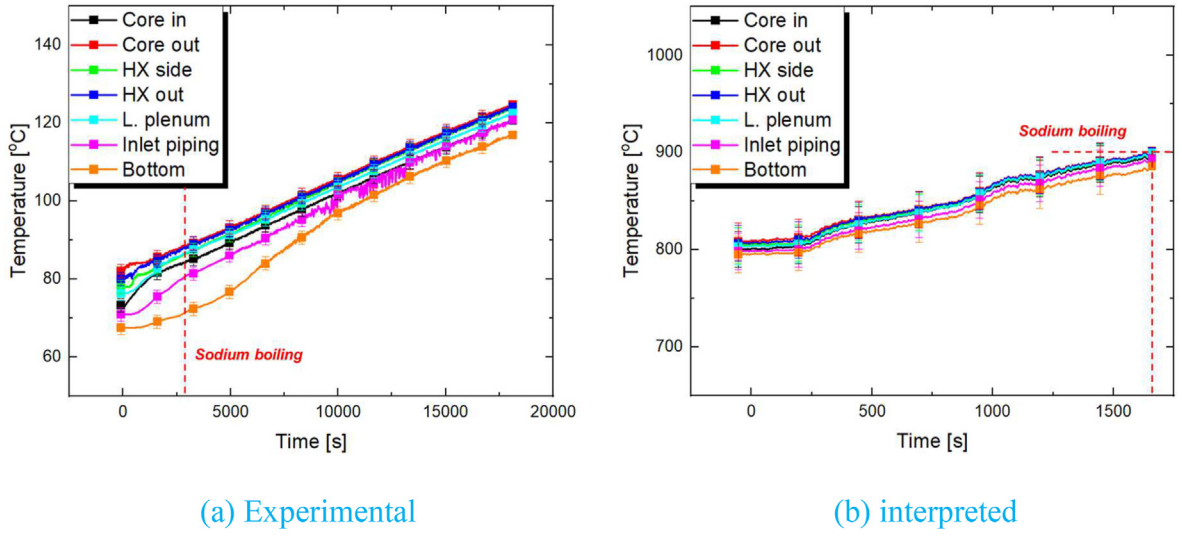

Fig. 13. Transient summary, 1.1 → 10.0 %.

shown in interpreted data. Regard to the initial state of the interpreted data, it showed significantly higher temperature than that of the previous case. During data interpretation, temperature difference was greatly increased between the air and wall due to higher air average temperature and heat flux. Temperature distribution inside of the pool was also negligible in this case. Sodium boiling was predicted at approximately 1,660 s. It was quite shorter time than that in the previous case, 25,100 s. The reasons for more than 10 times of the boiling time difference were temperature difference of the initial states and heat storage rate. 1.0 → 2.0 % case, the pool was approximately 750°C, while 800°C in 1.1 → 10.0 % case. Considering development of the RVACS performance with transient, in 1.0 → 2.0 % case, 2.0 % of the heat was given while 1.0–1.5 % of the heat was removed by the RVACS. Therefore, approximately 0.5–1.0 % of the heat imbalance made temperature increase. However, in 1.1 → 10.0 % case, 10.0 % of the heat was given while 1.0–1.5 % of the heat was removed. Finally, 8.5–9.0 % of the heat imbalance made temperature increase. Temperature increase rate of the interpreted data was approximately 6°C per 1,000 s and 60°C per 1,000 s, for 2.0 % and 10.0 %, respectively. Therefore, it was reasonable that sodium boiling prediction between two conditions showed more than 10 times of the difference.

In summary, sodium boiling time was predicted as 25,100 s and 1,660 s, for 1.0 → 2.0 %, and 1.1 → 10.0 %, respectively. Considering heat imbalance and accumulation, it was the reasonable results and the sodium boiling time was compared to that by the system code calculation in case of 1.0 → 2.0 %. For transient test benchmark using the TRACE code, a two-step simulation using a restart file was used. At first step, the phase 1 of the experiment was simulated. Thereafter, using its restart file and an input deck containing the conditions for phase 2, the rest of the experiment was simulated. In this paper, the 1.0 → 2.0 % condition was served as a benchmark data. Fig. 14 shows the result of the TRACE code benchmark, in terms of the heat removed through RVACS (simulated using an air channel in SINCRO-IT) and temperature versus time. The temperature at the IHX outlet and the bottom, was compared. The capability of TRACE code to simulate the experiment using the Wood's metal has confirmed by benchmarking the steady-state

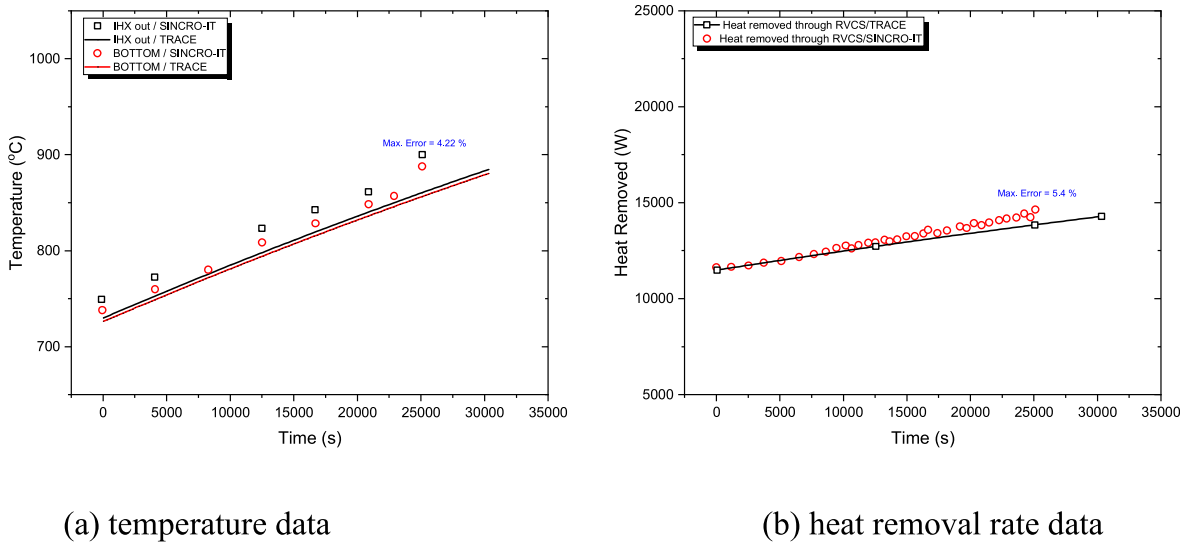

(a) temperature data (b) heat removal rate data

Fig. 14. Transient experiment benchmark summary, 1.0 → 2.0 % case.

experiment. In the transient experiment benchmarking, the interpreted results were served as a benchmark data. That is, the TRACE code benchmark was conducted in sodium-air condition. By doing so, not only the capability of TRACE code to predict the flow and heat transfer but also the verification of the interpretation method can be done.

The temperature comparison which is shown in (a) of the Fig. 14, indicated that the temperature inside the pool could also be predicted reasonably. The error of the predicted temperatures and the experimental values were less than 4.2 %. It can be found that the predicted temperatures were slightly less than that obtained from the experiment. The heat removed through the air cooling channel, is shown in (b) of the Fig. 14, and the result indicated that the TRACE code predicted the heat removal rate and its change along the time accurately, with an maximum error of 5.4 %. A slight discrepancy on the rate of change of the heat removal rate was observed at last seconds (around 25,000 s), yet it can be concluded that the TRACE code can predict not only natural circulation behavior inside the pool, but also the heat transfer though the air cooling system, until the sodium boiling occurred. The sodium boiling occurred approximately 30,300 s by TRACE. Through the transient experiment benchmark with sodium-air condition, although the radiation heat transfer was omitted, SINCRO-IT and its design showed its capability to simulate the original sodium-air system by scaled-down Wood's metal-air system. At the same time, the system code TRACE showed its capability to predict the RVACS performance during transient, with 4.2 % of error in temperature, and 5.4 % of error in heat removal rate in maximum.

4. Conclusions

To evaluate performance of the RVACS, SINCRO-IT was designed for integrated and transient experiments. There was a combination of the two different similarity laws for in- and ex-vessel, which was the most unique and important point in the present research. For the in-vessel natural circulation, Bo' based similarity law was applied, while Ishii's law was applied for the ex-vessel natural circulation. In terms of the heat transfer, both sides of the vessel showed good similarity. Regard to the time scales, which was the most important parameter for the integrated and transient experiments, were the same for both sides. The SINCRO-IT had 1.68 : 1 of the time scale, and 1 : 4 of the length scale compared to the prototype. Original working fluids: sodium and air, were simulated by Wood's metal and air.

Experimental data were translated into the that of the prototype, and it would be mainly discussed with two main safety parameters: the RV temperature and the sodium boiling. Under steady state, at 0.8 % of the decay heat, the RV temperature was violated creep temperature, while sodium boiling was predicted at 1.3 % of the decay heat. The system code showed good accordance with the interpreted of the simulating experiments. Regard to the transient experiments, the scenario was selected as an arbitrary re-criticality during RVACS only decay heat cooling, to guarantee the similarities. In case of 1.0 → 2.0 % case, the sodium boiled 25,100 s after the transient, while 1,660 s were predicted in 1.1 → 10.0 % case. System codes TRACE predicted sodium boiling at 30,100 in case of 1.0 → 2.0 % case. The maximum discrepancies between the experiment and system code until sodium boiling were 4.2 % and 5.4 %, in terms of temperature and heat removal rate, respectively. Through the comparison between the system code and experimental results, validity of the experimental and design methodology, and predictability of the RVACS performance of TRACE were validated at the same time.

From the design of the SINCRO-IT, the liquid metal to liquid metal simulating experiments were suggested and proven. The unique methodology, the combination of the two different similarity law was suggested for simulating experiment of the system including two or more domains. It was also validated by comparing with the system code TRACE. Therefore, the experimental results could be employed for the validation of the RVACS model, and the code could have potential to analyze various accident with the RVACS.

Declaration of competing interest

The authors declare that they have no known competing financial interests or personal relationships that could have appeared to influence the work reported in this paper.

Acknowledgment

This work was supported by the Basic Science Research Program (NRF- 2020M2A8A4022882, 2021M2D2A1A03048950) through the National Research Foundation of Korea (NRF) funded by the

Korea government, the Ministry of Science and ICT (MSIT).

Nomenclature

A	Area[m^2]
Bo'	Modified Boussinesq number[1].
c_p	Specific heat[J/kg.K]
D	Diameter[m]
d	Channel width[m]
F	Pressure drop coefficient[1].
f	Muddy's friction factor[1].
Gr'	Modified Grashof number[1].
g	Gravitational acceleration[m/s^2]
h	Convective heat transfer coefficient[$W/m^2.K$]
K	Minor loss coefficient[1].
L	Length[m]
L_{h-c}	Length between thermal centers[m]
L_{heater}	Length of the hot fluid section[m]
P	Pressure[Pa]
Ri	Richardson number[1].
Q	Heat generation[W]
Q_0	Volumetric heat generation[W/m3]
q"	Heat flux[W/m2]
St	Stanton number[1].
T	Temperature[K]
t	time [s]
u	Velocity[m/s]
x	Cartesian coordinates[m]
α	thermal diffusivity[m^2/s]
β	Volumetric expansion coefficient[1/K]
δ	Kronecker delta[1].
ν	Kinematic viscosity[m^2/s]
ρ	Density[kg/m^3]
c	cold side
f	fluid
h	hot side
I	Indicator of discretization
i,j,k	i,j,k-th coordinates
R	ratio of between the model and prototype
ref	reference properties
s	solid
*	non-dimensionalized quantities

References

[1] T.L. Schulz, Westinghouse AP1000 advanced passive plant, Nuclear Engineering and Design 236 (2006) 1547–1557.

[2] K.M. Kim, D.H. Lee, I.C. Bang, Analysis of natural circulation behaviors and flow instability of passive containment cooling system design for advanced PWR using MARS-KS code, International Journal of Heat and Mass Transfer 147 (2020), 118982.

[3] M. Sawada, H. Arikawa, N. Mizoo, Experiment and analysis of natural convection characteristics in the experimental fast reactor JOYO, Nuclear Engineering and Design 120 (1990) 341–347.

[4] H. Mochizuki, Analyses of decay heat removal tests with PRACS and DRACS of a sodium loop using the NETFLOW++ code, Nuclear Engineering and Design 322 (2017) 345–359.

[5] T. Mihara, E. Hourcade, F. Curnier, B. Farges, J.-F. Dirat, et al., in: ASTRID Nuclear Island Design : Advances in French-Japanese Joint Team Development of Decay Heat Removal Systems. ICAPP 2016 - International Congress on Advances in Nuclear Power Plants, Apr 2016. San Francisco, United States. cea-02442366.

[6] J. Yoo, J. Chang, J.Y. Lim, J.S. Cheon, T.H. Lee, S.K. Kim, K.L. Lee, H.K. Joo, Overall system description and safety characteristics of prototype gen IV sodium cooled fast reactor in Korea, Nuclear Engineering and Technology 48 (2016) 1059–1070.

[7] A. Alemberti, V. Smirnov, C.F. Smith, M. Takahashi, Overview of lead cooled fast reactor activities, Progress in Nuclear Energy 77 (2014) 300–307.

[8] F. Giannetti, D.V.D. Mario, A. Naviglio, G. Caruso, Thermal-hydraulic analysis of an innovative decay heat removal system for lead-cooled fast reactors, Nuclear Engineering and Design 305 (2016) 168–178.

[9] K.V. Tichelen, G. Kennedy, F. Mirelli, A. Marino, A. Toti, D. Rozzia, E. Cascioli, S. Keijers, P. Planquart, Advanced liquid-metal thermal-hydraulic Research for MYRRHA, Nuclear Technology 206 (2020) 150–163.

[10] S. Grewal, E. Gluekler, Water simulation of sodium reactors, Chemical Engineering Communications 17 (1982) 343–360.

[11] Y. Eguchi, H. Takeda, T. Koga, N. Tanaka, K. Yamamoto, Quantitative prediction of natural circulation in an LMFR with a similarity law and a water test, Nuclear Engineering and Design 178 (1997) 295–307.

[12] M.H. Lee, D.W. Jerng, I.C. Bang, Experimental validation of simulating natural circulation of liquid metal using water, Nuclear Engineering and Technology 52 (2020) 1963–1973.

[13] H. Hoffman, K. Hain, K. Marten, H. Ohira, K. Rust, D. Weinberg, The status of thermal-hydraulic studies on the decay heat removal by natural convection using RAMONA and NEPTUN models, in: Proceedings of the 4th International Topical Meeting on Nuclear Thermal Hydraulics, Operation and Safety, Taipei, Taiwan, 1994.

[14] D. Weinberg, K. Rust, H. Hoffman, Overview report of RANONA-NEPTUN program on passive decay heat removal, No. FZKA–5667. Forschungszentrum Karlsruhe GmbH Technik und Umwelt (Germany), Inst. fuer Angewandte Thermo-und Fluiddynamik, 1996.

[15] A. Ono, A. Kurihara, M. Tanaka, H. Oshima, H. Kamide, Study on Reactor Vessel Coolability of Sodium Cooled Fast Reactor under Severe Accident Condition Water Experiments Using a Scale Model, 2017. ICAPP 2017, Fukui and Kyoto, Japan.

[16] A. Bar-Cohen, W.M. Rohsenow, Thermally optimum spacing of vertical, natural convection cooled, parallel plates, Journal of Heat Transfer 106 (1984) 116–123.

[17] R.A. Wirtz, R.J. Stutzman, Experiments on free convection between vertical plates with symmetric heating, Journal of Heat Transfer 104 (1982) 501–507.

[18] X. Cheng, U. Müller, Turbulent natural convection coupled with thermal radiation in large vertical channels with asymmetric heating, International Journal of Heat and Mass Transfer 41 (1998) 1681–1692.

[19] J. Heineman, M. Kraimer, P. Lotters, D. Pedersen, R. Stewart, J. Tessier, Experimental and Analytical Studies of a Passive Shutdown Heat Removal System for Advanced LMRs, Argonne National Laboratory CONF-880532-10, USA, 1988.

[20] S.Y. Kim, D.H. Shin, C.S. Kim, G.C. Park, H.K. Cho, Flow visualization experiment in a two-side wall heated rectangular duct for turbulence model assessment, Nuclear Engineering and Design 341 (2019) 284–296.

[21] K.M. Kim, J.H. Hwang, S. Wongwises, D.W. Jerng, H.S. Ahn, Design of A scale-down experimental model for SFR reactor vault cooling system performance analyses, Nuclear Engineering and Technology 52 (2020) 1611–1625.

[22] K.M. Kim, D.H. Nguyen, G.H. Shim, D.W. Jerng, H.S. Ahn, Experimental study of turbulent air natural convection in open-ended vertical parallel plates under asymmetric heating conditions, International Journal of Heat and Mass Transfer 159 (2020), 120135.

[23] K.M. Kim, S.T. Lim, S.H. Kim, H. Kim, D.W. Jerng, H.S. Ahn, Transition phenomena of natural convection of the air in an asymmetrically heated vertical channel with a damper, International Journal of Heat and Mass Transfer 183 (2022), 122196.

[24] G. Wu, M. Jin, J. Chen, Y. Bai, Y. Wu, Assessment of RVACS performance for small size lead-cooled fast reactor, Annals of Nuclear Energy 77 (2015) 310–317.

[25] C. Choi, T. Jeong, S. An, Thermal-hydraulic analyses of passive reactor vault cooling system (RVCS) in PGSFR using MARS-LMR, Annals of Nuclear Energy 117 (2018) 333–342.

[26] S. Wang, D. Zhang, Y. Liu, C. Wang, S. Qiu, G. Su, W. Tian, An experiment-based validation of a system code for prediction of passive natural circulation in sodium-cooled fast reactor, International Journal of Energy Research 45 (2021) 12093–12109.

[27] G.H. Koo, S.H. Kim, S.K. Kim, N.H. Kim, J.H. Lee, C.G. Park, J.B. Kim, H.W. Kim, Y.S. Joo, NSSS Design and Validation of Prototype Gen-IV Sodium Cooled Fast Reactor, Mechanical Design of Prototype Gen-IV Sodium Cooled Fast Reactor, 2015. KAERI/RR–4048/2015, Korea, Republic of.

Further reading

[28] M. Ishii, Scaling laws for thermal-hydraulic system under single phase and two phase natural circulation, Nuclear Engineering and Design 81 (1984) 411–425.